frontiers | Frontiers in Physics

ORIGINAL RESEARCH
published: 27 June 2022
doi: 10.3389/fphy.2022.943744

# Te Film as a Saturable Absorber for the Mid-Infrared $Er^{3+}$-Doped ZBLAN Fiber Laser

*Min Zhang*, Liu Kang, Zhijian Ma, Peiguang Yan and Shaodong Hou*

*Key Laboratory of Optoelectronic Devices and Systems of Ministry of Education and Guangdong Province, College of Physics and Optoelectronic Engineering, Shenzhen University, Shenzhen, China*

We demonstrate a Q-switched $Er^{3+}$-doped ZBLAN fiber laser at 2.8 μm mid-infrared (mid-IR) region achieved by adopting Te as the saturable absorber mirror (SAM). The modulation depth and saturation intensity of the Te-SAM were measured to be ~7.2% and 10.81 MW/cm$^2$, respectively. Stable Q-switched laser pulses with the maximum pulse energy of 3.05 μJ and the minimum pulse width of 0.457 μs at the launched pump power of 4.51 W were obtained. Maximum average output power of 357 mW with repetition rate of 116.98 kHz were achieved. The signal-to-noise ratio (SNR) is 52 dB, which is higher than that of most 2.8 μm mid-infrared Q-switched fiber lasers reported so far. To the best of our knowledge, this is the first demonstration from a Q-switched fiber laser at 2.8 μm based on a Te-SAM.

**Keywords: Q-switched, $Er^{3+}$-doped, ZBLAN fiber, mid-infrared, saturable absorber mirror**



***Edited by:***
*Yufei Ma,*
*Harbin Institute of Technology, China*

***Reviewed by:***
*Xiaohui Li,*
*Shaanxi Normal University, China*
*Quandong Huang,*
*Guangdong University of Technology, China*

****Correspondence:***
*Min Zhang*
*zhangmin@szu.edu.cn*

***Specialty section:***
*This article was submitted to Optics and Photonics, a section of the journal Frontiers in Physics*

***Received:*** *14 May 2022*
***Accepted:*** *06 June 2022*
***Published:*** *27 June 2022*

***Citation:***
*Zhang M, Kang L, Ma Z, Yan P and Hou S (2022) Te Film as a Saturable Absorber for the Mid-Infrared $Er^{3+}$-Doped ZBLAN Fiber Laser. Front. Phys. 10:943744. doi: 10.3389/fphy.2022.943744*

## 1 INTRODUCTION

In recent years, mid-infrared lasers have received enormous attentions owing to their substantial applications in gas detection, remote sensing, spectroscopy, and biomedical surgery [1–6]. In contrast to continuous-wave ones, mid-IR Q-switched fiber lasers feature the distinct advantages of high reliability, outstanding beam quality, excellent surface-to-volume ratio, and great efficiency, which promote their practical applications [7]. Up to present, semiconductor saturable absorption mirrors (SESAMs), $Fe^{2+}$:ZnSe crystals, black phosphorus (BP), graphene and topological insulators (Tls) have been widely applied as saturable absorbers (SAs) in mid-IR passively Q-switched fluoride fiber lasers at 2.8 μm [8–21]. SESAMs have controlled modulation depth but the limited bandwidths make them not suitable for broadband pulsed lasers. $Fe^{2+}$:ZnSe crystals exhibit a large saturable absorption cross section and high damage threshold (~2 J/cm$^2$). However, $Fe^{2+}$:ZnSe crystals usually have the characteristics of complex preparation process, relatively expensive cost and narrow absorption band. BP exhibits a large modulation depth but it is easy to oxidize in the ambient air. Despite graphene is characterized by zero bandgap, the modulation depth of single-layer graphene is only about 2.3% [22–28].

In this letter, we report, as far as we know, a 2.8 μm mid-IR $Er^{3+}$-doped ZBLAN Q-switched fiber laser using Te saturable absorber mirror (SAM) for the first time. The obtained maximum output power and pulse energy are 357 mW and 3.05 μJ, respectively. The results facilitate the application range of Te-SAM based Q-Switched fiber laser as well as affirm that Te is expected to be an effective SAM of mid infrared fiber laser.

## 2 PREPARATION AND CHARACTERIZATION OF TE SATURABLE ABSORBER MIRROR

In our experiment, Te-SAM were prepared by a common magnetron-sputtering deposition (MSD) method. First of all, Te target and gold mirror were simultaneously placed in a magnetron sputtering

chamber, the vacuum pressure of the chamber was pulled to about $10^{-3}$ Pascal. Then, the stimulated ionized Argon ions rapidly bombarded the Te target. Thus, the Te atoms was slowly deposited on the gold mirror. An uniformly arranged tellurium film could be obtained on the surface of the gold mirror after deposition, the coating time was set to 1 min. The Raman shift spectra were measured by a Raman spectrometer (LabRAM HR Evolution, HORIBA Scientific, 514 nm emission) with an excitation wavelength of 514 nm. **Figure 1A** presented the surface of Te film, measured by a scanning electron microscope with a dense and well-distributed shape. The cross-section image of Te SAM with cold field emission scanning electron microscope was displayed in **Figure 1B**, where the thickness of the Te film was approximately measured to be 40.7 nm. The thickness of the film was measured by the atomic force microscope (AFM) in **Figures 1A,C** highly uniform surface can be observed. As shown in **Figure 1D**, the Raman spectra of Te film showed two obvious peaks located at 122 $cm^{-1}$ and 140 $cm^{-1}$, consistenting with the peaks reported in previous literature [29, 30], implying that the thin film used in the experiment has high purity. The nonlinear absorption of Te-coated fiber was studied by using a 2.8 μm ultrafast light source (pulse width: 350 fs, repetition rate: 68 MHz) built by our laboratory, and the experimental results were depcited in **Figure 2A**. The data conformed to the following equation:

$$T(I) = 1 - \Delta T \cdot \exp(-I/I_{sat}) - T_{ns}$$

Where $T(I)$ is the power-dependent transmission, $I$ is the incident intensity, $\Delta T$ is the modulation depth, $T_{ns}$ is the non-saturable loss, and $I_{sat}$ is the saturation peak intensity. The modulation depth $\Delta T$, saturation peak intensity $I_{sat}$ and non-saturable loss $T_{ns}$ were ~7.2%, ~10.81 MW/$cm^2$, ~76.1% respectively. The lower modulation depth can be improved by changing the thickness of Te film. To determine the composition of the magnetron deposition film, X-ray photoelectron spectroscopy (XPS) measurements (Thermo Fisher Scientific, K-Alpha+) were performed, and the data obtained were shown in **Figures 2B,C**, all calibrated with a C1s peak of 284.8 eV. The fully binding energy spectroscopic scan shows a low energy resolution, and all peaks were related to the expected elements except for the weak C1s peak caused by air pollution. **Figure 2B** shows the high resolution XPS spectra of the characteristic peaks of the Te sample for determining chemical states and elemental bonds. $Te3d_{3/2}$ and $Te3d_{5/2}$ peaks were found at 583.45 and 573.14 eV, which closely matched the chemical state of Te.

## 3 EXPERIMENTAL SETUP

**Figure 3** depicts the schematic diagram of the passively Q-switched $Er^{3+}$-doped ZBLAN fiber laser. The pump was provided by a commercial 976 nm fiber coupled semiconductor laser (MChlight, Shenzhen) which can achieve higher pump efficiency with a maximum output power of 9 W, a core/cladding diameter of 105/125 μm and a numerical aperture of 0.22 NA. Two uncoated $CaF_2$ plano-convex lenses (L1 = 40 mm, T = 98.8% at 976 nm, T = 99.5% at 2.8 μm, L2 = 40 mm, T = 99.5% at 2.8 μm) were used to collimate and focus the pump beam into a 3 m long double-cladding 7 mol%-doped Er:ZBLAN fiber with a core diameter of 15 μm, 1st cladding diameter of 240*260 μm, 2nd cladding

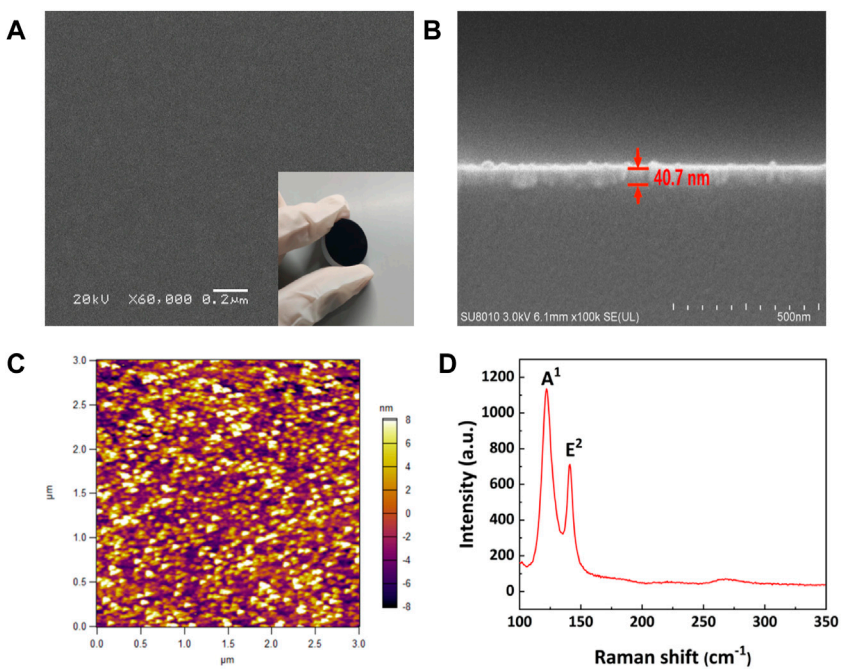


**FIGURE 1 | (A)** SEM image for surface topography and **(B)** the lateral surface of the Te-SAM. **(C)** AFM image. **(D)** Raman shift spectrum.

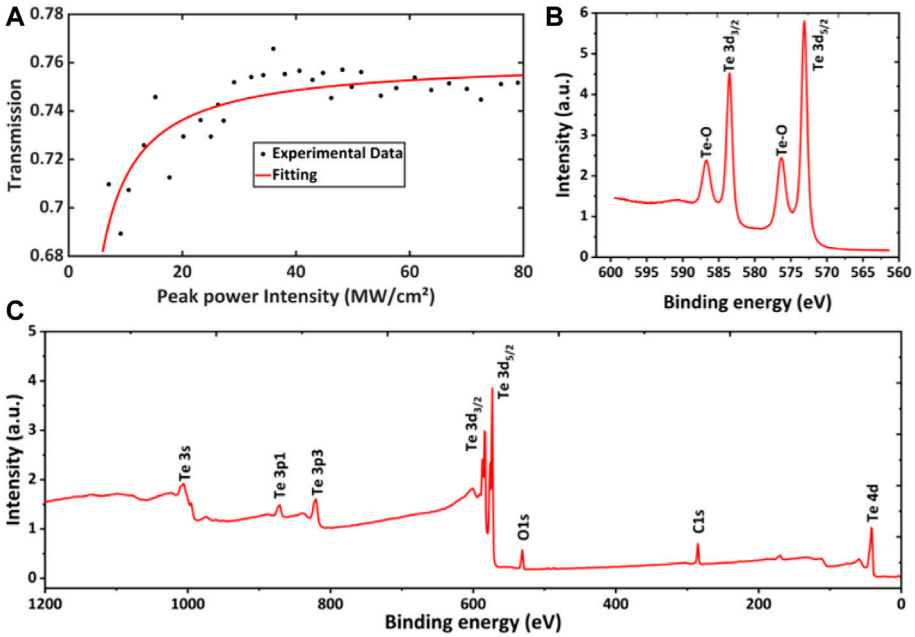


**FIGURE 2 | (A)** Nonlinear saturable absorption curve of the Te-SAM. **(B)** XPS core level spectrum of Te 3d. **(C)** Full XPS spectrum of fabricated Te film.

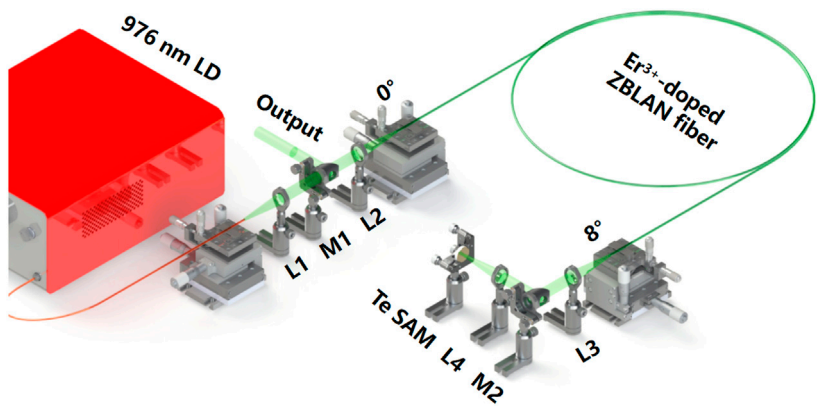


**FIGURE 3 |** The schematic of the Q-switched Er:ZBLAN fiber laser.

diameter of 290 μm, and a numerical aperture (NA) of 0.12. Between the two $CaF_2$ plano-convex lenses, a dichroic mirror M1 with high reflectance of 94% at around 2.8 μm and high transmittance of 97.6% at 976 nm was placed at a 45° angle of incidence surface to couple out the 2.8 μm laser. The front end of the fiber was angle-cleaved at 0° to provide ~4% Fresnel reflection, while the other fiber end was cleaved at angle of 8° to suppress parasitic oscillation. Two uncoated $CaF_2$ plano-convex lenses (L3 = 40 mm, T = 98.8% at 976 nm, T = 99.5% at 2.8 μm, L4 = 40 mm, T = 99.5% at 2.8 μm) were used to collimate and focus the 2.8 μm laser beam from the angle-cleaved fiber end onto the Te-SAM. Then another dichroic mirror M2 (T > 95% @ 976 nm & R > 99% @ 2.8 μm) was placed at 45° to couple out the surplus 976 nm pump light. The average output power of the cavity was acquired by a power meter (Laserpoint) together with an IR bandpass filter (Thorlabs, FB2750-500) placed before the detector which was used to remove the background light. An detector with a response time of ~2 ns was connected to a 4-GHz bandwidth digital oscilloscope (ROHDE & SCHWARZ, RTO2044) to measured the pulse temporal trains. The optical spectrum was monitored by a optical spectrum analyzer (YOKOGAWA, AQ6376) with a minimum scanning resolution of 0.1 nm. A RF spectrum analyzer (ROHDE & SCHWARZ, FSWP) with a scanning range of 1 MHz–8 GHz was utilized to analyze the radio frequency (RF) spectrum.

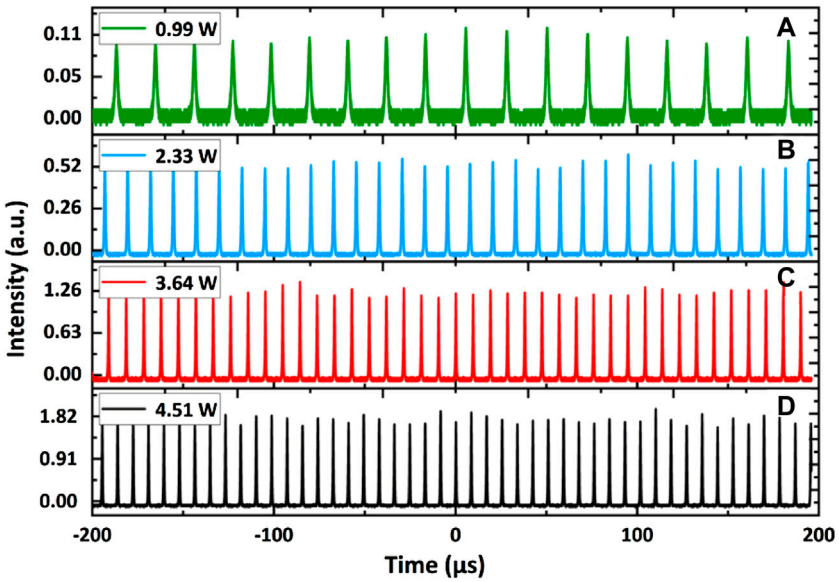


**FIGURE 4 |** Typical Q-switched pulse trains at the launched pump powers of **(A)** 0.99 W, **(B)** 2.33 W, **(C)** 3.64 W and **(D)** 4.51 W, respectively.

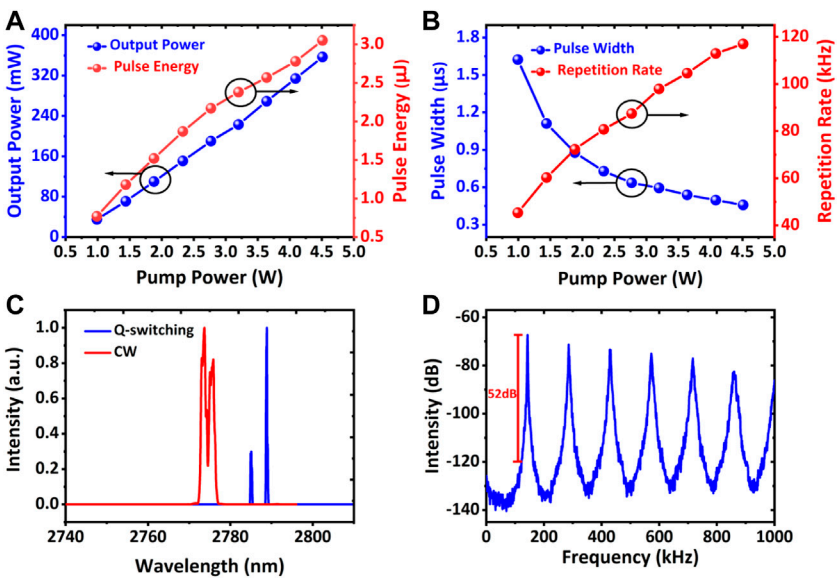


**FIGURE 5 | (A)** Average output power and pulse energy. **(B)** Repetition rate and pulse width of the Q-switched Er:ZBLAN fiber laser as a function of the pump power. **(C)** Spectrum of Q-switching and CW operation. **(D)** Fundamental repetition rate with RBW of 100 Hz.

## 4 EXPERIMENTAL RESULTS AND DISCUSSION

**Figure 4** presents the Q-switched pulse sequences and pulses profiles under different pump powers. **Figure 5A** displays the measured output power and calculated pulse energy of Q-switched pulses as a function of the launched pump power. It can be achieved in the broad pump power range of 0.99–4.51 W with an output power of 35–357 mW at a slope efficiency of 9.2% and a pulse energy of 0.77–3.05 μJ. **Figure 5B** shows the pulse repetition rate and pulse width as a function of the launched pump power. As expected, with the increase of the launched pump power, the repetition rate increased and the pulse width decreased. When the pump power increased within the above range, the pulse repetition rate increasd from 45.34 to 116.98 kHz, and the pulse width decreased from 1.624 to 0.457 μs. In the system, CW began to oscillate when the launched pump power was about 0.87 W. A self-starting Q-switching train was observed

with a pulse width of 1.62 μs and a repetition rate of 45.34 kHz when the launched pump power exceeded the threshold of 0.99 W, as shown in **Figure 4A** and **Figure 5B**. As presented in **Figure 4B** and **Figure 5B**, stable Q-switching can be maintained by slightly increasing the launched pump power to 2.33 W and the pulse width was 0.73 μs at a repetition rate of 80.75 kHz. When the launched pump power continued to increase, the Q-switching operation can be maintained. Typical Q-switched pulse waveforms at launched pump power of 3.64 and 4.51 W are shown in **Figures 4C,D**. Their pulse width were 0.54 and 0.457 μs, respectively. At the same time, the corresponding repetition rates were 104.63 and 116.98 kHz, respectively. The optical and RF spectrum were measured at the maximum pump power of 4.51 W. **Figure 5C** depicts the pulse spectrum of the laser under continuous-wave (CW) centered at 2,775 nm and Q-switching operation centered at 2,782.35 nm, the recording range is 70 nm (from 2,740 to 2,810 nm). The signal-to-noise ratio (SNR) of the RF spectrum is measured to be 52 dB at a resolution bandwidth (RBW) of 100 Hz in a 1000-kHz scanning span, indicating a stable Q-switching regime, as shown in **Figure 5D**. When the launched pump power was higher than 4.51 W, the Q-switching pulse began to become unstable but Q-switching can still be realized by focusing.

## 5 CONCLUSION

In conclusion, we have presented a mid-infrared 2.8 μm Q-switched Er:ZBLAN fiber laser using Te as a Q-switcher for the first time to the best of our knowledge. The Te-SAM has a modulation depth of ~7.2% and saturation intensity of 10.81 MW/cm$^2$, respectively. Stable Q-switched pulse trains were obtained with a repetition rate of 116.98 kHz and a pulse width of 0.457 μs at the maximum launched pump power. The maximum pulse energy of 3.05 μJ, average output power of 357 mW were achieved, respectively. The signal-to-noise ratio (SNR) is 52 dB, which is higher than most known 2.8 μm mid infrared Q-switched fiber lasers. The research results not only indicate that Te is an excellent SA material for stable pulses generation in mid-IR Q-switched fiber lasers but also provides a cost-effective method for the preparation of mid-infrared SAM.

## DATA AVAILABILITY STATEMENT

The original contributions presented in the study are included in the article/supplementary material, further inquiries can be directed to the corresponding author.

## AUTHOR CONTRIBUTIONS

MZ guided the experiments, LK drafted the manuscript, ZM fabricated Te saturable absorber, PY and SH revised the text. All the authors contributed the conception and design of the experimental study.

## FUNDING

This work was supported by the National Natural Science Foundation of China 61935014 and the Science and Technology Innovation Commission of Shenzhen under Grants 20200812163234001.

## REFERENCES

1. Töpfer T, Petrov KP, Mine Y, Jundt D, Curl RF, Tittel FKRoom-temperature Mid-infrared Laser Sensor for Trace Gas Detection. *Appl Opt* (1997) 36(30): 8042–9. doi:10.1364/ao.36.008042
2. Walsh BM, Lee HR, Barnes NPMid Infrared Lasers for Remote Sensing Applications. *J Lumin* (2016) 169:400–5. doi:10.1016/j.jlumin.2015.03.004
3. Ma Y, Feng W, Qiao S, Zhao Z, Gao S, Wang YHollow-core Anti-resonant Fiber Based Light-Induced Thermoelastic Spectroscopy for Gas Sensing. *Opt Express* (2022) 30(11):18836–44. doi:10.1364/OE.460134
4. Lang Z, Qiao S, Ma YAcoustic Microresonator Based In-Plane Quartz-Enhanced Photoacoustic Spectroscopy Sensor with a Line Interaction Mode. *Opt Lett* (2022) 47(6):1295–8. doi:10.1364/ol.452085
5. Ma Y, He Y, Tong Y, Yu X, Tittel FKQuartz-tuning-fork Enhanced Photothermal Spectroscopy for Ultra-high Sensitive Trace Gas Detection. *Opt Express* (2018) 26(24):32103–10. doi:10.1364/oe.26.032103
6. Ma Y, Hu Y, Qiao S, Lang Z, Liu X, He Y, et al.Quartz Tuning forks Resonance Frequency Matching for Laser Spectroscopy Sensing. *Photoacoustics* (2022) 25: 100329. doi:10.1016/j.pacs.2022.100329
7. Fortin V, Bernier M, Bah ST, Vallée R30 W Fluoride Glass All-Fiber Laser at 294 μm. *Opt Lett* (2015) 40(12):2882–5. doi:10.1364/ol.40.002882
8. Li JF, Luo HY, He YL, Liu Y, Zhang L, Zhou KM, et al.Semiconductor Saturable Absorber Mirror Passively Q-Switched 2.97μm Fluoride Fiber Laser. *Laser Phys Lett* (2014) 11:065102. doi:10.1088/1612-2011/11/6/065102
9. Zhu G, Zhu X, Balakrishnan K, Norwood RA, Peyghambarian NFe2+:ZnSe and Graphene Q-Switched Singly Ho3+-Doped ZBLAN Fiber Lasers at 3 μm. *Opt Mater Express* (2013) 3(9):1365–77. doi:10.1364/ome.3.001365
10. Li J, Luo H, Zhai B, Lu R, Guo Z, Zhang H, et al.Black Phosphorus: a Two-Dimension Saturable Absorption Material for Mid-infrared Q-Switched and Mode-Locked Fiber Lasers. *Sci Rep* (2016) 6(1):30361. doi:10.1038/srep30361
11. Qin Z, Xie G, Zhang H, Zhao C, Yuan P, Wen S, et al.Black Phosphorus as Saturable Absorber for the Q-Switched Er:ZBLAN Fiber Laser at 28 μm. *Opt Express* (2015) 23(19):24713–8. doi:10.1364/oe.23.024713
12. Frerichs C, Unrau UBPassive Q-Switching and Mode-Locking of Erbium-Doped Fluoride Fiber Lasers at 2.7 Mm. *Opt Fiber Technol* (1996) 2(41): 358–66. doi:10.1006/ofte.1996.0041
13. Wang X, Xu J, Sun Y, Feng W, You Z, Sun D2 and 3 Mm Passively Q-Switched Bulk Pulse Laser Based on a $MoS_2$/graphene Heterojunction. *Laser Phys Lett* (2017) 15(1):15801. doi:10.1088/1612-202x/aa9158
14. Zhou L, Wei C, Wang D, Chi H, Le Zheng L, Jiang S, et al.Ti3C2Tx Nanosheets for High-Repetition-Rate Wideband-Tunable Q-Switched Fiber Laser Around 3 μm. *IEEE Photon Technol Lett* (2021) 33(10):515–8. doi:10.1109/lpt.2021.3072651
15. Li X, Yu X, Sun Z, Yan Z, Sun B, Cheng Y, et al.High-power Graphene Mode-Locked Tm/Ho Co-doped Fiber Laser with Evanescent Field Interaction. *Sci Rep* (2015) 5:16624. doi:10.1038/srep16624
16. Liu JS, Li XH, Guo YX, Qyyum A, Shi ZJ, Feng TC, et al.SnSe 2 Nanosheets for Subpicosecond Harmonic Mode-Locked Pulse Generation. *Small* (2019) 15(38):1902811. doi:10.1002/smll.201902811

17. Zhao Y, Guo P, Li X, Jin ZUltrafast Photonics Application of Graphdiyne in the Optical Communication Region. *Carbon* (2019) 149:336–41. doi:10.1016/j.carbon.2019.04.075
18. Feng J, Li X, Zhu G, Wang QJEmerging High-Performance SnS/CdS Nanoflower Heterojunction for Ultrafast Photonics. *ACS Appl Mater Inter* (2020) 12(38):43098–105. doi:10.1021/acsami.0c12907
19. Li X, Zhang C, Wang Y, Liu J, Liu JHydrazone Organic Compound with R2C═N-NR Substructure for Ultrafast Photonics. *J Phys Chem C* (2020) 124(41):22638–45. doi:10.1021/acs.jpcc.0c05434
20. Li XH, Guo YX, Ren Y, Peng JJ, Liu JS, Wang C, et al.Narrow-bandgap Materials for Optoelectronics Applications. *Front Phys* (2022) 17(1):13304. doi:10.1007/s11467-021-1055-z
21. Zhang C, Liu J, Gao Y, Li X, Lu H, Wang Y, et al.Porous Nickel Oxide Micron Polyhedral Particles for High-Performance Ultrafast Photonics. *Opt Laser Technol* (2022) 146:107546. doi:10.1016/j.optlastec.2021.107546
22. Ning S, Feng G, Dai S, Zhang H, Zhang W, Deng L, et al.Mid-infrared Fe2+:ZnSe Semiconductor Saturable Absorber Mirror for Passively Q-Switched Er3+-Doped ZBLAN Fiber Laser. *AIP Adv* (2018) 8(2):025121. doi:10.1063/1.5012847
23. Chen W, Lyu Y, Shi H, Kang Z, Zhang H, Qin G, et al.Mid-Infrared Q-Switched and Mode-Locked Fiber Lasers at 2.87 Mm Based on Carbon Nanotube. *IEEE J Selected Top Quan Electron* (2019) 25(4):1100206. doi:10.1109/JSTQE.2019.2899015
24. Guo C, Wei J, Yan P, Luo R, Ruan S, Wang J, et al.Mode-locked Fiber Laser at 2.8 μm Using a Chemical-Vapor-Deposited WSe2 Saturable Absorber Mirror. *Appl Phys Express* (2020) 13:012013. doi:10.7567/1882-0786/ab6031
25. Lee BC, Kim CM, Jang HK, Lee JW, Joo MK, Kim GTDegradation Pattern of Black Phosphorus Multilayer Field–effect Transistors in Ambient Conditions: Strategy for Contact Resistance Engineering in BP Transistors. *Appl Surf Sci* (2017) 419:637–41. doi:10.1016/j.apsusc.2017.04.126
26. Khirat M, Lazab M, Bettahar N, Rached DFirst-principles Calculations of the Band Ordering Conversion in theLaxSc2−xRuPbcompounds. *Solid State Commun* (2018) 276:14–8. doi:10.1016/j.ssc.2018.03.018
27. Tabert CJ, Carbotte JPMagnetization of the Metallic Surface States in Topological Insulators. *J Phys Condens Matter* (2014) 27(1):015008. doi:10.1088/0953-8984/27/1/015008
28. Xie HY, Chang R, Leung PTDipole Emission Characteristics Near a Topological Insulator Sphere Coated with a Metallic Nanoshell. *Results Phys* (2021) 23:104014. doi:10.1016/j.rinp.2021.104014
29. Sun J, Nie Q, Wang X, Dai S, Zhang X, Bureau B, et al.Structural Investigation of Te-Based Chalcogenide Glasses Using Raman Spectroscopy. *Infrared Phys Technol* (2012) 55:316–9. doi:10.1016/j.infrared.2012.03.003
30. Min J, Liang X, Chen J, Wang D, Li H, Zhang JInvestigation of Te Inclusions in CdZnTe Crystalline Material Using Raman Spectroscopy and IR Techniques. *Vacuum* (2012) 86:1003–6. doi:10.1016/j.vacuum.2011.11.009

**Conflict of Interest:** The authors declare that the research was conducted in the absence of any commercial or financial relationships that could be construed as a potential conflict of interest.

**Publisher's Note:** All claims expressed in this article are solely those of the authors and do not necessarily represent those of their affiliated organizations, or those of the publisher, the editors and the reviewers. Any product that may be evaluated in this article, or claim that may be made by its manufacturer, is not guaranteed or endorsed by the publisher.